ISO Observations of the dusty quasar BR1202-0725

K.J. Leech,[1] L. Metcalfe,[1] B. Altieri,[2]

[1] *ISO Data Centre, Astrophysics Division, Space Science Department of ESA, Villafranca del Castillo, P.O. Box 50727,*
28080 Madrid, Spain
[2] *XMM-Newton Data Centre, Astrophysics Division, Space Science Department of ESA, Villafranca del Castillo, P.O. Box 50727,*
28080 Madrid, Spain

date

ABSTRACT

We present mid- and far-IR photometry of the high-redshift (z=4.69) dusty quasar BR1202-0725. The quasar was detected in the near-IR, at a flux level (0.7±0.2 mJy) consistent with an average Radio-Quiet Quasar at it's redshift. Only upper limits for the emission were obtained in the far-IR. These upper limits, when combined with data from ground-based telescopes, are the first direct evidence for a turn-over in the far-IR emission and hence confirm that a black-body dominates the SED at FIR wavelengths. This black-body is most probably cool dust, constrained to have a temperature below 80K, for a β of 1.5.

Key words: galaxies : active – galaxies : photometry – infrared : galaxies – quasars : individual : BR1202-0725

1 INTRODUCTION

It came as a surprise when groups working with IRAS data, e.g. Soifer et al. (1984) & Lawrence et al. (1986), discovered galaxies with bolometric luminosities equivalent to those of quasars but emitting predominantly in the infra-red wavelength region. Even more surprising was the discovery by Rowan-Robinson et al. (1991) of IRAS FSC 10214+4724, a galaxy at a redshift of z=2.29 with an apparent IR luminosity of 4×10^{14} L$_\odot$. While F10214+4724 has turned out to be gravitationally lensed (Eisenhardt et al. 1996), leading to a lower luminosity of 2×10^{13} L$_\odot$, it is still of extreme luminosity.

Five high-redshift radio-quiet QSO's were selected, primarily from an APM catalogue, by McMahon et al. (1994) because their similarity to F10214+4724 in redshift and overall properties made them natural objects in which to look for IR-emission from dust. BR1202-0725 (see figure 1 for a DSS image of the quasar and surrounding field), at a redshift of 4.69, was the only one to be detected at 1.25 mm with IRAM. Assuming the detection was due to dust and that the dust had a single temperature (80K was assumed), McMahon et al. (1994) derived a dust mass of the order of 4×10^8 M$_\odot$, a considerable amount of dust to exist at such an early epoch. If the far-IR spectrum of BR1202-0725 is similar to that of F10214+4724 then it has an IR luminosity of the order of 10^{14}L$_\odot$, making it one of the most luminous objects in the universe.

Later IR observations of this object by Isaak et al. (1994) at 450, 800 & 1100 μm, and by Benford et al. (1999) at 350 microns, supported a slightly lower dust temperature of 68K and 50±7 K respectively, although none of these ob-

servations saw the turnover of the emission to confirm that it comes from a black-body. Indeed, its spectral index of 2.7±0.4 between 1100 and 800μm, calculated by Isaak et al., does not formally rule out synchrotron-emission, although a spectral index above 2.5 is difficult to explain by anything other than cool dust.

The detection of CO emission from approximately 1×10^{11}M$_\odot$ of molecular hydrogen (comparable to that in a present-day luminous galaxy) by Ohta et al. (1996) and Omont et al. (1996b), and the detection by Omont et al. (1996b) of a close companion also containing large amounts of molecular gas, further reinforced the idea that the galaxy was undergoing a large burst of star formation, possibly interaction triggered.

2 OBSERVATIONS AND DATA REDUCTION

2.1 Observing Strategy

The observations of BR1202-0725 had two goals: to try and detect the turnover in the far-IR emission; and to detect the near-IR emission from the continuum to better determine the underlying power-law. Early predictions from Isaak et al. (1994) were for flux densities in the $100 - 200\mu m$ range to reach of the order of 100 mJy, depending on dust temperature. We therefore proposed to make observations through the wideband C90 and C160 filters (centred at 90 and 170 μm) of the ISOPHOT instrument (Lemke et al. 1996) onboard ESA's Infrared Space Observatory (ISO, Kessler et al. 1996). It was hoped these two far-IR observations would lie either side of the peak of the emission.
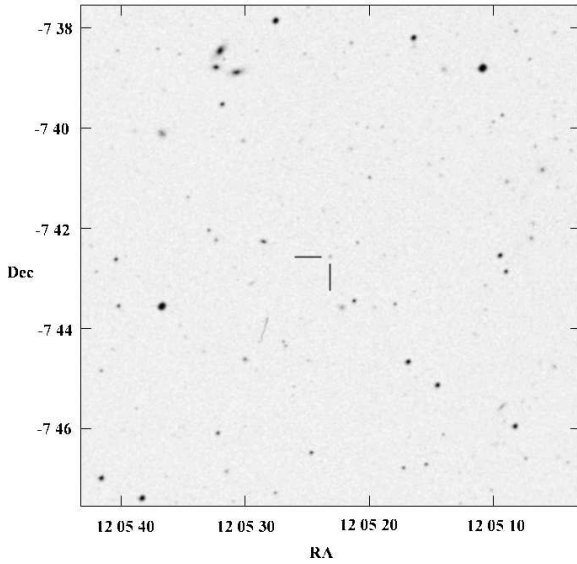
Figure 1. The field around the quasar BR 1202-0725, taken from the DSS. The quasar is in the middle of the field and is indicated. The scale is consistent with figure 3.

Table 1. ISO observations, taken on 14 July 1996.

Observation Mode	TDT number	Wavelength μm	Filter	Exposure secs
CAM01	24002102	8–15	LW10	348
PHT32	24002103	90	C90	606
PHT32	24002101	170	C160	2696

The ISOCAM instrument, described in Cesarsky et al. (1996), was used to obtain a single observation through the LW10 ($8-15\ \mu m$) filter with the aim of detecting the near-IR emission of BR1202-0725. A normal RQQ quasar with the redshift of BR1202-0725 would have a flux of approximately 1mJy in this band, and the ISOCAM observation was therefore planned to reach that sensitivity by employing the microscanning mode.

2.2   Observations

Observations, listed in Table 1, were performed on July 14 1996. The ISOCAM observation was taken in microscanning mode, with the field-of-view of the instrument scanned over the object of interest in a 3×3 raster pattern. The detector was read out every 2.1 seconds, leading to redundancy in the dataset. The redundancy is used to distinguish glitches and other artifacts from valid sources. The ISOPHOT observations were taken as PHT32 rasters of size 3×4. The ISOCAM (Siebenmorgen et al. 1999) and ISOPHOT (Laureijs et al. 2000) Handbooks give complete descriptions of these observing modes.

2.3   Data reduction

2.3.1   CAM Data Reduction

The data was sliced and dark corrected in the standard way (Delaney 2000), making use of a time-dependent dark correction. A thorough first-order deglitching was performed using an iterative sigma-clipping method (Metcalfe et al. in prep).

No correction was made at this stage for the effects of responsive transients as the existing correction algorithms can adversely affect the S/N for very faint sources. The transient correction was instead made at the end of the data reduction by applying an appropriate scaling factor. This factor was established by transient correcting reference sources identified for this purpose in representative data sets.

Dedicated faint-source processing followed essentially the method described in Altieri et al. (1998) and Metcalfe et al. (in prep).

Long-term baseline drifts were removed by smoothing (via median filtering) the time-history of each individual detector pixel, as sampled by the hundreds of readouts made during the observation, and then subtracting the smoothed baseline from the nominal history. The images recorded at the several raster positions were organised into a cube so that all samples of a given sky-position line-up. For each sky position, this sky-position-vector is then sigma-clipped to give a second-order deglitching which has been found to be extremely effective in removing residual glitches. It should be noted that first-order deglitching acts on the time-history of a detector pixel, as it moves over the sky during a raster. Second-order deglitching acts on the history of samples of each sky position, and so takes implicit advantage of the sampling redundancy of the raster measurement technique. The two deglitching steps are therefore highly complementary. Following this deglitching stage the raster mosaic was constructed straightforwardly from the raster-position-images and standard aperture photometry could be performed on the resulting map.

In order to calibrate the aperture photometry the data were re-processed after inserting a set of fake sources into the raw data cube. These consisted of theoretical model PSFs matched to the optical configuration in use. By performing aperture photometry on these fake sources in a manner identical to that used for the actual source any flux-altering effects of the complex data-reduction algorithm could be calibrated.

The fake-source insertion operation was repeated for a range of fake-source brightnesses. In this way the source strength in ADUgs (ADU per gain per second) in the raw data, corresponding to a given source strength in the reduced map, was determined.

At this point it was only necessary to scale the source strength in the raw data for the effects of responsive transients (as described above) and to apply the standard calibration scaling factor relating ADUgs to incident mJy for each CAM filter (Siebenmorgen et al. 1999), in order to arrive at an estimate of the flux of the target source.

2.3.2   ISOPHOT Data Reduction

The ISOPHOT P32 data was reduced using the PHOT Interactive Analysis (PIA) package including a pre-release version of P32 processing routines developed by R. Tuffs (Tuffs
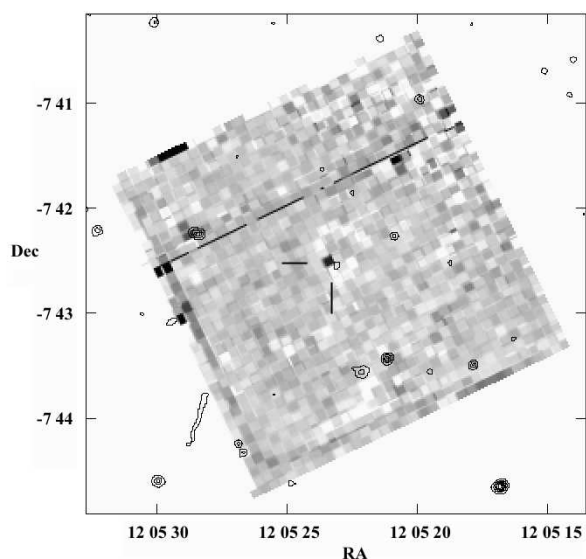
Figure 2. The ISOCAM image overplotted with contours from a DSS2 red image. The quasar is in the centre of the image, with the black line above being the missing column 24. There is a slight shift between the two images of approximately 5″. This offset is not significant as the uncertainty in the ISOCAM astrometry due to the wheel positioning jitter is greater than this. The position of the quasar is marked.
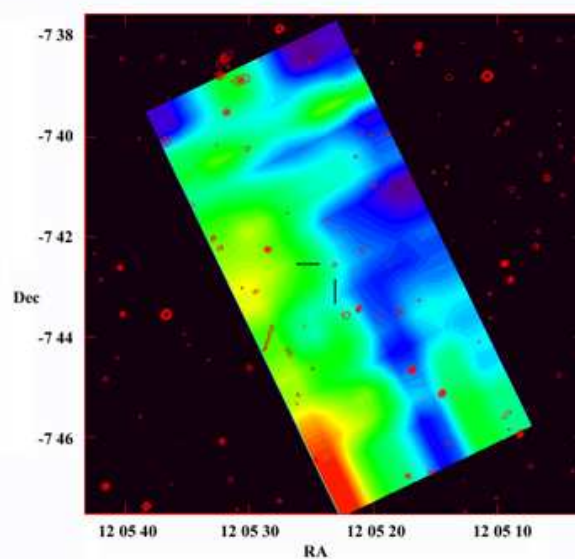

Figure 3. The $170\mu m$ ISOPHOT map. The quasar is located in the centre of the image but has not been detected by ISOPHOT. Its position is marked. (A colour version of this image is available at the MNRAS website.)

et al. in prep.). Initial data processing (ERD to SCP) used the new P32 processing routines, with the later processing (SCP to AAP) using the standard processing routines. Default values for the reduction parameters were used in both the old and new routines.

Maps were generated using the Trigrid interpolation and the first quartile normalization flat-fielding methods.

3 RESULTS

In the ISOCAM dataset, see Figure 2, BR1202-0725 was detected with a flux of 0.7 mJy. Deriving the scatter in photometry of ten randomly placed apertures near the centre of the image produces a 1σ value of 0.07 mJy, while the results of the simulations give a (random plus systematic) uncertainty of 0.2 mJy. We therefore take a value of 0.7±0.2 mJy for the flux from this object in the 8–15 μm wavelength region. The background flux was determined to be 1.06±0.1 mJy per sq.arcsec (45±4 MJy sr^{-1}), consistent with the typical background predictions for CAM LW10 given in the user manual.

Other surrounding sources (visible on the DSS image) are also present in the ISOCAM image. As they are not in the centre of the image the observation was not optimised for them, leading to a higher uncertainty on their detections, and we therefore do not quote fluxes for them.

No object was detected at the position of the quasar in either the $90\mu m$ or $170\mu m$ datasets. The ISOPHOT $170\mu m$ map is shown in figure 3. The effective noise in both maps

was derived by moving a box the size of one C100 or C200 array pixel over the two maps (avoiding the outer parts of the maps) and converting to Jy. This produced 1 sigma noise values of 16 and 15 mJy at 90 and $170\mu m$ – effectively the 3 sigma upper limit for both maps is 50 mJy.

Combined results of this and other papers are presented in Table 2. Figure 4 shows the IR data, along with a greybody spectrum at a temperature of 68K. This was derived using the method outlined in Benford et al. (1999), i.e.

$$S_\nu = B_\nu \Omega (1 - exp(-\tau))$$

with $\tau = (\nu/\nu_0)^\beta$, where $\nu_0 = 2.4$ THz, the critical frequency at which the source becomes optically thin, and taking $\beta = 1.5$. The current data does not support the temperature of 50K, with the other parameters, presented in Benford et al. (1999). It is, however, consistent with the higher temperature of 68K as given in Isaak et al. (1994). The maximum temperature allowed by the $170\mu m$ upper limit is 80K, although then the fit to the longer wavelength data becomes poor.

Figure 5, shown as normalised L_ν against ν, extends the previous figure to include the 6cm data. It can be compared with the average spectrum for a Radio-Quiet Quasar given in either Figure 10 of Elvis et al. (1994) or Figure 7 of Polletta et al. (2000). If we approximately normalise the fluxes of BR1202-0725 at 6cm and R to those of the average RQQ the $15\mu m$ datapoint is also in agreement, whereas the $350 - 800$ μm fluxes from BR1202-0725 are higher than the average RQQ, indicating the presence of cool dust in this quasar.

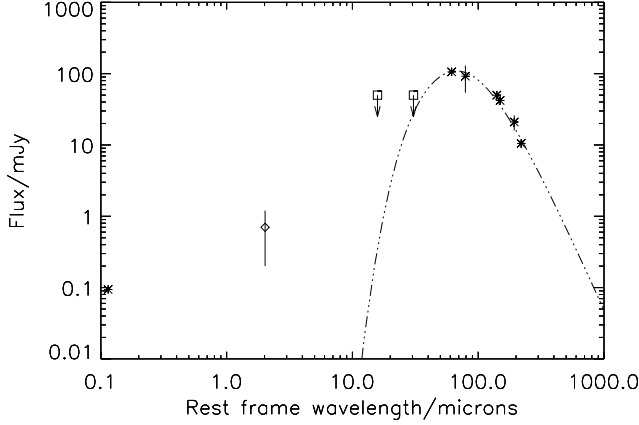**Figure 4.** Data points from Table 2 plotted with a black-body of temperature 68K. The ISOCAM datapoint is plotted as a diamond, the ISOPHOT 3σ upper limits are plotted as squares and observations with other instruments are plotted as asterisks. The 68K black-body is shown as a dash-dot line.
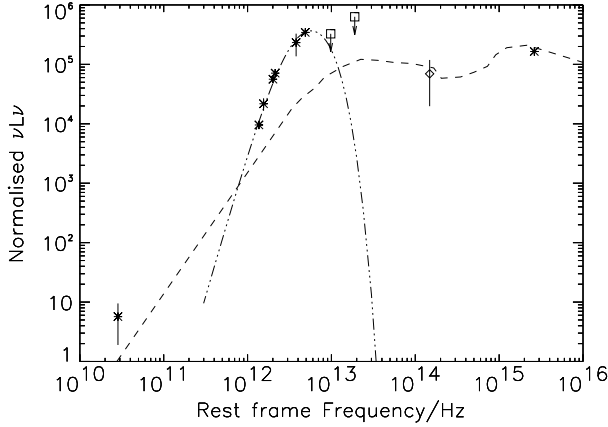

Figure 5. All data points from Table 2 plotted as relative luminosity against frequency. The ISOCAM datapoint is plotted as a diamond, the ISOPHOT 3σ upper limits are plotted as squares and observations with other instruments are plotted as asterisks. The 68K black-body is shown as a dash-dot line, and the average RQQ SED from Elvis et al. (1994) is shown as a dashed line. The $15\mu m$ flux of BR1202-0725 is consistent with the average RQQ, whereas it exhibits an excess of emission at the far-IR wavelengths.

4   CONCLUSIONS

We have detected the distant, dusty quasar BR1202-0725 in the near-IR and obtained upper-limits for the flux at two far-IR wavelengths. The upper-limits for the flux levels at 90 and $170\mu m$, when combined with the previous ground-based measurements, are consistent with the far-IR and sub-mm being emitted from a grey-body, most probably arising from dust. The maximum temperature allowed by the $170\mu m$ upper limit is 80 K, while the probable temperature is 68K.

The near-IR flux level of 0.7 ± 0.2 mJy at $11.5\mu m$ is at

Table 2. BR1202-0725 fluxes.

Observed Wavelength μm	Rest Wavelength μm	Flux mJy	Precision mJy
0.65[1]	0.114	0.094	–
11.5	2.02	0.7	0.2
90	15.8	< 50[5]	
170	30.6	< 50[5]	
350[2]	61.5	106	7
450[3]	79.1	92	38
800[3]	141	50	7
1100[3]	193	21	5
1250[1]	220	10.5	1.5
1250[4]	220	12.59	2.28
60000[1]	10500	0.3	0.2

1. McMahon et al. (1994).
2. Benford et al. (1999).
3. Isaak et al. (1994).
4. Omont et al. (1996a).
5. These are 3σ upper limits.

a level consistent with with originating in a normal quasar at the distance of BR1202-0725.

REFERENCES

Altieri B., Metcalfe L., Ott S., Biviano A, Blommaert J., Delaney M., 1998. ISOCAM Faint Source report (16/Nov/1998) http://www.iso.vilspa.esa.es/users/expl_lib/CAM/fs_report. ps.gz
Benford D. J., Cox P., Omont, A., Phillips, T. G., McMahon, R. G., 1999, ApJ 518, L65.
Cesarsky C.J. et al., 1996, A&A, 315, L32
Delaney M., 2000, ISOCAM Interactive Analysis User's Manual, Version 4.0 http://www.iso.vilspa.esa.es/manuals/CAM/ users_manual_v4_0.ps.gz
Eisenhardt P.R., Armus L., Hogg D.W., Soifer B.T., Neugebauer G., Werner M.W., 1996, ApJ 461, 72.
Elvis, M., et al., 1994, ApJS 95, 1.
Isaak K.G., McMahon R.G., Hills R.E., Withington S., 1994. MNRAS, 269, L28.
Kessler M.F. et al., 1996. A&A, 315, L27

Laureijs R., Klaas U., Richards P.J., Schulz B., Abraham P., 2000, ISO Handbook Volume V (PHT), SAI/99-069/Dc, http://www.iso.vilspa.esa.es/manuals/HANDBOOK/V/pht_hb/

Lawrence A. Walker D., Rowan-Robinson M., Leech K. J., Penston M. V., 1986. MNRAS 219, 687.

Lemke D. et al., 1996, A&A 315, L64

McMahon R. G., Omont A., Bergeron J., Kreysa E., Haslam C. G. T., 1994. MNRAS, 267, L9.

Ohta K., Yamada Y., Nakanishi K., Kohno K., Aklyama M., Kawabe R., 1996. Nat. 382, 426.

Omont A., McMahon R. G., Cox P., Kreysa E., Bergeron J., Pajot F., Storrie-Lombardi L. J., 1996. A&A 315, 1.

Omont A., Petitjean, P., Guilloteau, S., McMahon R. G., Solomon, P.M., Pecontal, E., 1996. Nat. 382, 428.

Polletta M., Courvoisier T.J.-L., Hooper E.J., Wilkes B.J., 2000. A&A 362, 75.

Rowan-Robinson M., et al., 1991. Nat. 351, 719.

Siebenmorgen R., Blommaert J., Sauvage M., Starck J-L., 1999, ISO Handbook Volume III (CAM), SAI-99-057/Dc, http://www.iso.vilspa.esa.es/users/expl_lib/CAM_top.html

Soifer T., et al., 1984. ApJ 278, L71.